



**HAL**  
open science

# Reverting the mode of action of the mitochondrial FOF1-ATPase by *Legionella pneumophila* preserves its replication niche

Pedro Escoll, Lucien Platon, Mariatou Dramé, Tobias Sahr, Silke Schmidt, Christophe Rusniok, Carmen Buchrieser

## ► To cite this version:

Pedro Escoll, Lucien Platon, Mariatou Dramé, Tobias Sahr, Silke Schmidt, et al.. Reverting the mode of action of the mitochondrial FOF1-ATPase by *Legionella pneumophila* preserves its replication niche. 2021. pasteur-03242972

**HAL Id: pasteur-03242972**

**<https://pasteur.hal.science/pasteur-03242972>**

Preprint submitted on 31 May 2021

**HAL** is a multi-disciplinary open access archive for the deposit and dissemination of scientific research documents, whether they are published or not. The documents may come from teaching and research institutions in France or abroad, or from public or private research centers.

L'archive ouverte pluridisciplinaire **HAL**, est destinée au dépôt et à la diffusion de documents scientifiques de niveau recherche, publiés ou non, émanant des établissements d'enseignement et de recherche français ou étrangers, des laboratoires publics ou privés.



Distributed under a Creative Commons Attribution - NonCommercial - NoDerivatives 4.0 International License

1  
2 **Reverting the mode of action of the mitochondrial F<sub>0</sub>F<sub>1</sub>-ATPase by**  
3 ***Legionella pneumophila* preserves its replication niche**  
4

5  
6 Pedro Escoll <sup>1,2,\*</sup>, Lucien Platon <sup>1,2,3,+,‡</sup>, Mariatou Dramé <sup>1,2,4,‡</sup>, Tobias Sahr <sup>1,2</sup>,  
7 Silke Schmidt <sup>1,2,5</sup>, Christophe Rusniok <sup>1,2</sup> & Carmen Buchrieser <sup>1,2,\*</sup>  
8

9  
10 <sup>1</sup>*Institut Pasteur, Biologie des Bactéries Intracellulaires and*, <sup>2</sup>*CNRS UMR 3525, 75024 Paris,*  
11 *France*, <sup>3</sup>*Faculté des Sciences, Université de Montpellier, 34095 Montpellier, France*, <sup>4</sup>*Université de*  
12 *Paris, 75013 Paris, France*, <sup>5</sup>*Sorbonne Université, Collège doctoral, 75005 Paris, France*  
13

14  
15 **Keywords:** *Legionella pneumophila*, OXPHOS, mitochondria, F<sub>0</sub>F<sub>1</sub>-ATPase, mitochondrial  
16 membrane potential, cell death, macrophages  
17

18  
19 <sup>+</sup> Present address: Institut Pasteur, Génétique du Paludisme et Résistance, Paris, France

20 <sup>‡</sup> These authors contributed equally to the work  
21

22  
23 \* For correspondence:

24 Pedro Escoll and Carmen Buchrieser  
25 Institut Pasteur, Biologie des Bactéries Intracellulaires  
26 28, rue du Dr. Roux, 75724 Paris Cedex 15, France  
27 Tel: (33-1)-44-38-95-40  
28 Fax: (33-1)-45-68-87-86  
29 E-mail: [pescoll@pasteur.fr](mailto:pescoll@pasteur.fr) and [cbuch@pasteur.fr](mailto:cbuch@pasteur.fr)  
30

31 **ABSTRACT**

32 *Legionella pneumophila*, the causative agent of Legionnaires' disease, a severe pneumonia,  
33 injects *via* a type-IV-secretion-system (T4SS) more than 300 proteins into macrophages, its  
34 main host cell in humans. Certain of these proteins are implicated in reprogramming the  
35 metabolism of infected cells by reducing mitochondrial oxidative phosphorylation (OXPHOS)  
36 early after infection. Here we show that despite reduced OXPHOS, the mitochondrial  
37 membrane potential ( $\Delta\psi_m$ ) is maintained during infection of primary human monocyte-derived  
38 macrophages (hMDMs). We reveal that *L. pneumophila* reverses the ATP-synthase activity of  
39 the mitochondrial F<sub>0</sub>F<sub>1</sub>-ATPase to ATP-hydrolase activity in a T4SS-dependent manner, which  
40 leads to a conservation of the  $\Delta\psi_m$ , preserves mitochondrial polarization and prevents  
41 macrophage cell death. Analyses of T4SS effectors known to target mitochondrial functions  
42 revealed that *LpSpl* is partially involved in conserving the  $\Delta\psi_m$ , but not LncP and MitF. The  
43 inhibition of the *L. pneumophila*-induced "reverse mode" of the F<sub>0</sub>F<sub>1</sub>-ATPase collapsed the  
44  $\Delta\psi_m$  and caused cell death in infected cells. Single-cell analyses suggested that bacterial  
45 replication occurs preferentially in hMDMs that conserved the  $\Delta\psi_m$  and showed delayed cell  
46 death. This direct manipulation of the mode of activity of the F<sub>0</sub>F<sub>1</sub>-ATPase is a newly identified  
47 feature of *L. pneumophila* allowing to delay host cell death and thereby to preserve the bacterial  
48 replication niche during infection.

49

## 50 INTRODUCTION

51 Beyond their essential role in cellular bioenergetics, mitochondria are integrated into diverse  
52 signaling pathways in eukaryotic cells and perform various signaling functions, such as immune  
53 responses or cell death, as they play crucial roles in the regulation of apoptosis (Bock and Tait,  
54 2020). Thus mitochondria are targeted by several intracellular bacteria during infection to  
55 modulate their functions to the bacterial advantage (Spier et al., 2019). One of these bacteria is  
56 *Legionella pneumophila*, the causative agent of Legionnaires' disease. We have shown  
57 previously that this pathogen targets mitochondrial dynamics during infection of primary  
58 human monocyte-derived macrophages (hMDMs) by injecting type IV secretion system (T4SS)  
59 effectors such as MitF, leading to a fragmented mitochondrial network *via* the recruitment of  
60 the host fission protein DNM1L to the mitochondrial surface (Escoll et al., 2017b). Importantly,  
61 *Legionella* induced mitochondrial fragmentation at early time points such as 5 hours post-  
62 infection (hpi), when bacterial replication has not started yet, and in the absence of cell death  
63 signs. The fragmentation of mitochondrial networks provoked a T4SS-dependent reduction of  
64 mitochondrial respiration in *Legionella*-infected macrophages, evidencing a functional  
65 connection between mitochondrial dynamics and mitochondrial respiration (Escoll et al.,  
66 2017b).

67 Mitochondrial respiration results from coupling the activity of five complexes in the electron  
68 transport chain (ETC) at mitochondrial cristae. In this process, the reduced coenzymes NADH  
69 and FADH<sub>2</sub> generated at the mitochondrial matrix by the tricarboxylic acid (TCA) cycle are  
70 oxidized at Complexes I and II where their electrons are extracted to energize the mitochondrial  
71 ETC (Nolfi-Donagan et al., 2020). The sequential transit of these electrons through Complexes  
72 I, III and IV allows to pump protons from the matrix to the intermembrane space (IMS) and at  
73 Complex IV, diatomic oxygen O<sub>2</sub> serves as the terminal electron acceptor and H<sub>2</sub>O is formed.  
74 The increased concentration of protons [H<sup>+</sup>] at the IMS, compared to [H<sup>+</sup>] at the matrix,  
75 generates the mitochondrial membrane potential ( $\Delta\psi_m$ ). This is necessary to produce ATP  
76 by fueling the rotation of Complex V, the mitochondrial F<sub>0</sub>F<sub>1</sub>-ATPase, in a process termed  
77 oxidative phosphorylation, OXPHOS (Nolfi-Donagan et al., 2020). Our previous studies  
78 determined that at 5 hpi *L. pneumophila*, by altering mitochondrial dynamics, reduced  
79 OXPHOS as well as the cellular ATP content in hMDMs in a T4SS-dependent manner (Escoll  
80 et al., 2017b).

81 Why *L. pneumophila* and other species of intracellular bacteria reduce mitochondrial  
82 OXPHOS during infection of host cells remains a matter of debate (Escoll and Buchrieser,

83 2018; Russell et al., 2019). As intracellular bacteria can obtain resources only from host cells,  
84 it has been suggested that halting mitochondrial OXPHOS during infection might benefit  
85 pathogenic bacteria by redirecting cellular resources, such as glycolytic or TCA intermediates,  
86 to biosynthetic pathways that might sustain intracellular bacterial replication instead of fueling  
87 mitochondria (Escoll and Buchrieser, 2018; Russell et al., 2019). For instance, it has been  
88 shown that *Mycobacterium tuberculosis* redirects pyruvate to fatty acid synthesis and  
89 *Chlamydia trachomatis* subverts the pentose phosphate pathway to increase the synthesis of  
90 nucleotides for its own intracellular growth (Siegl et al., 2014; Singh et al., 2012). On the other  
91 hand, upon sensing bacterial lipopolysaccharides, macrophages redirect mitochondrial TCA  
92 intermediates, such as citrate or succinate, to drive specific immune functions such as the  
93 production of cytokines or the generation of antimicrobial molecules (Escoll and Buchrieser,  
94 2019; Russell et al., 2019; O'Neill and Pearce, 2016). Thus, while these metabolic shifts, which  
95 are redirecting resources from mitochondria to the cytoplasm should be activated in  
96 macrophages to develop their antimicrobial functions, they could also benefit intracellular  
97 bacteria, as more resources would be available in the cytoplasm for bacterial growth.  
98 Importantly, reduction of OXPHOS may lead to decreased  $\Delta\psi_m$  and ATP production at  
99 mitochondria, which are events that trigger the activation of cell death programs. How  
100 intracellular bacteria withdraw OXPHOS, deal with the subsequent  $\Delta\psi_m$  drop and host cell  
101 death but manage to preserve their host cell to conserve their replication niche is a question that  
102 remains poorly understood.

103 To answer this question, we monitored the evolution of mitochondrial polarization during  
104 infection of hMDMs by *L. pneumophila*, and showed that in the absence of OXPHOS,  
105 *L. pneumophila* regulates the enzymatic activity of the mitochondrial F<sub>0</sub>F<sub>1</sub>-ATPase during  
106 infection. This allows maintaining the  $\Delta\psi_m$  and delays cell death of infected hMDMs in a T4SS-  
107 dependent manner. Our results identified a new virulence mechanism of *L. pneumophila*,  
108 namely the manipulation of the mitochondrial F<sub>0</sub>F<sub>1</sub>-ATPase to preserve the integrity of infected  
109 host cells and thereby the maintenance of the bacterial replication niches.

## 110 RESULTS

### 111 **Despite *L. pneumophila*-induced Reduction of Mitochondrial Respiration, the** 112 **Mitochondrial Membrane Potential Is Maintained**

113 We have previously shown that *L. pneumophila* strain Philadelphia JR32 impairs mitochondrial  
114 respiration during infection (Escoll et al., 2017b). Here we analyzed *L. pneumophila* strain Paris  
115 (Lpp) to learn whether this is a general characteristic of *L. pneumophila* infection. We infected

116 hMDMs with Lpp WT or a T4SS-deficient mutant ( $\Delta dotA$ ) for 6 hours and analyzed their  
117 mitochondrial function compared to uninfected hMDMs by using a cellular *respiratory control*  
118 *assay* in living cells (Brand and Nicholls, 2011; Connolly et al., 2018). This assay determines  
119 oxygen consumption rate (OCR) in basal conditions and during the sequential addition of  
120 mitochondrial respiratory inhibitors. OCR variations observed indicate how mitochondrial  
121 respiration is functioning in a cell population (Figure 1A and S1A). Our results showed that  
122 basal respiration is significantly reduced ( $p < 0.0001$ ) in WT-infected hMDMs compared to  
123  $\Delta dotA$ - and non-infected hMDMs (Figure 1A and 1B). This indicates that  $O_2$  consumption,  
124 which is predominantly driven by ATP turnover and the flow of  $H^+$  to the matrix through the  
125 mitochondrial  $F_0F_1$ -ATPase, is severely impaired in WT-infected hMDMs. Further analysis of  
126 OCR changes upon addition of oligomycin, an inhibitor of the mitochondrial  $F_0F_1$ -ATPase,  
127 indicated that the rate of mitochondrial respiration coupled to ATP synthesis is highly reduced  
128 in WT-infected hMDMs, compared to  $\Delta dotA$ - or non-infected cells. Other respiratory  
129 parameters such as proton leak were also reduced in WT-infected macrophages (Figure 1A,  
130 S1A and S1B). Subsequent addition of an uncoupler to create a  $H^+$  short-circuit across the inner  
131 mitochondrial membrane (IMM), such as FCCP, allowed measuring the maximum respiration  
132 rate and the spare respiratory capacity, revealing that both were severely impaired in WT-  
133 infected cells compared to  $\Delta dotA$ - and non-infected hMDMs (Figure 1A, S1A and S1B).  
134 Finally, inhibition of the respiratory complexes I and III with rotenone and antimycin A,  
135 respectively, measured  $O_2$  consumption driven by non-mitochondrial processes, such as  
136 cytoplasmic NAD(P)H oxidases, which showed similar levels of non-mitochondrial  $O_2$   
137 consumption in all infection conditions (Figure 1A, S1A and S1B).

138 Taken together, our results indicated that several mitochondrial respiration parameters were  
139 severely altered during infection with Lpp-WT, including respiration coupled to ATP  
140 production. Importantly, some of the respiratory parameters measured that are oligomycin-  
141 sensitive were reduced in Lpp-WT-infected hMDMs but not in  $\Delta dotA$ -infected cells, suggesting  
142 that the mitochondrial  $F_0F_1$ -ATPase activity may be altered during *L. pneumophila* infection in  
143 a T4SS-dependent manner.

144 The transition of electrons across mitochondrial ETC complexes allows the extrusion of  $H^+$   
145 from the matrix to the IMS generating a  $H^+$  circuit where the mitochondrial  $F_0F_1$ -ATPase is the  
146 dominant  $H^+$  re-entry site during active ATP synthesis by OXPHOS. In cellular steady-state  
147 conditions, extrusion and re-entry  $H^+$  fluxes across mitochondrial membranes are balanced  
148 (Brand and Nicholls, 2011). Therefore, any exogenous alteration of ATP turnover and/or  $F_0F_1$ -

149 ATPase activity influences this H<sup>+</sup> circuit and might be reflected in  $\Delta\psi_m$  levels. Thus, we  
150 decided to quantify the  $\Delta\psi_m$  in infected cells. We developed a miniaturized *high-content* assay  
151 based on kinetic measurements of TMRM fluorescence in non-quenching conditions (10nM),  
152 where TMRM fluorescence in mitochondria is proportional to the  $\Delta\psi_m$  (Connolly et al., 2018;  
153 Duchen et al., 2003). This assay allowed to measure changes in the  $\Delta\psi_m$  at the single-cell level  
154 and in thousands of living cells during the course of infection (Figure 1C). Image analysis  
155 showed that the  $\Delta\psi_m$  slightly increased in Lpp-WT-, Lpp- $\Delta dotA$ - and non-infected cell  
156 populations during the first hours of infection (1-3 hpi), and progressively decreased during the  
157 time-course with no differences between the infection conditions (Figure 1D). Single-cell  
158 analyses (Figure 1E and S1C) showed that Lpp-WT-, Lpp- $\Delta dotA$ - and non-infected single  
159 hMDMs showed a wide range of  $\Delta\psi_m$  values at any time-point (Figure S1C) with no significant  
160 differences between them at 6 hpi (Figure 1E). Thus, despite a significant reduction of  
161 OXPPOS the  $\Delta\psi_m$  was maintained in infected cells, suggesting that *L. pneumophila*  
162 manipulates the mitochondrial ETC to conserve the  $\Delta\psi_m$  of hMDMs in the absence of  
163 OXPPOS.

#### 164 ***L. pneumophila* Infection Induces the “Reverse Mode” of the Mitochondrial F<sub>0</sub>F<sub>1</sub>-ATPase** 165 **in a T4SS-depended Manner**

166 The mitochondrial F<sub>0</sub>F<sub>1</sub>-ATPase is a fascinating molecular machine that rotates clockwise  
167 when it works in the “forward mode”, synthesizing ATP by using the  $\Delta\psi_m$  generated by the H<sup>+</sup>  
168 circuit (Figure 2A, left). It can also rotate counter-clockwise when it works in the “reverse  
169 mode”. In this case, it hydrolyzes ATP to maintain  $\Delta\psi_m$  in the absence of OXPPOS (Figure  
170 2A, right). As our results showed that *L. pneumophila* highly reduced OXPPOS, likely by an  
171 alteration of the F<sub>0</sub>F<sub>1</sub>-ATPase activity, while the  $\Delta\psi_m$  was conserved, we investigated in which  
172 activity mode the F<sub>0</sub>F<sub>1</sub>-ATPase worked during *Legionella* infection. A widely used method to  
173 investigate the directionality of the F<sub>0</sub>F<sub>1</sub>-ATPase in intact cells is to monitor changes in  $\Delta\psi_m$   
174 after the addition of F<sub>0</sub>F<sub>1</sub>-ATPase inhibitors, such as oligomycin or DCCD (Connolly et al.,  
175 2018; Gandhi et al., 2009). These inhibitors block both modes of function, thus if the F<sub>0</sub>F<sub>1</sub>-  
176 ATPase is working in the “forward mode” the  $\Delta\psi_m$  will increase after adding the inhibitor, as  
177 the inhibition of the H<sup>+</sup> flux to the matrix through the ATPase leads to an accumulation of H<sup>+</sup>  
178 at the IMS (Figure 2B, left). If  $\Delta\psi_m$  decreases after ATPase inhibition, the F<sub>0</sub>F<sub>1</sub>-ATPase works  
179 in the “reverse mode”, since now H<sup>+</sup> cannot translocate to the IMS to maintain the  $\Delta\psi_m$  (Figure  
180 2B, right). Here, we used the aforementioned TMRM high-content assay to monitor the  $\Delta\psi_m$  in  
181 living hMDMs at 6 hpi, when OXPPOS is impaired and  $\Delta\psi_m$  is maintained.

182 First, we recorded a baseline and then added medium as a control. As expected, this did not  
183 alter  $\Delta\psi_m$  in any infection condition (Figure 2C and 2D). However, the addition of FCCP  
184 completely depolarized mitochondria, leading to an abrupt drop of  $\Delta\psi_m$  in Lpp-WT-, Lpp-  
185  $\Delta dotA$ - and non-infected hMDMs (Figure 2C and 2E), demonstrating that this assay can  
186 monitor changes in the  $\Delta\psi_m$  simultaneously in hundreds of infected cells. To analyze whether  
187 the F<sub>0</sub>F<sub>1</sub>-ATPase worked in the synthase (forward) or the hydrolase (reverse) mode we added  
188 oligomycin (Figure 2F) or DCCD (Figure 2G) to the infected cells. The  $\Delta\psi_m$  increased in non-  
189 infected or  $\Delta dotA$ -infected hMDMs, which suggested that the ATPase worked in the “forward  
190 mode” in these infection conditions. In contrast, the addition of oligomycin to Lpp-WT-infected  
191 hMDMs had no effect on the  $\Delta\psi_m$  (Figure 2F), while addition of DCCD decreased the  $\Delta\psi_m$   
192 (Figure 2G). Thus, our results indicate that the F<sub>0</sub>F<sub>1</sub>-ATPase worked in the “forward mode” in  
193 non-infected or  $\Delta dotA$ -infected macrophages, whereas the F<sub>0</sub>F<sub>1</sub>-ATPase worked in the “reverse  
194 mode” during infection of hMDMs with the WT strain. This suggests that the induction of the  
195 “reverse mode” depends on the action of T4SS effector(s).

### 196 **The T4SS Effector *LpSPL* Participates in the Induction of the “Reverse Mode” of the** 197 **Mitochondrial F<sub>0</sub>F<sub>1</sub>-ATPase During Infection**

198 Among the more than 300 bacterial effectors that *L. pneumophila* injects into host cells through  
199 its T4SS (Mondino et al., 2020), three have been shown to target mitochondrial structures or  
200 functions. LncP is a T4SS effector targeted to mitochondria that assembles in the inner  
201 mitochondrial membrane (IMM) and seems to transport ATP across mitochondrial membranes  
202 (Dolezal et al., 2012). The effector *LpSpl* (also known as LegS2) was suggested to target  
203 mitochondria (Degtyar et al., 2009), the endoplasmic reticulum (ER, (Rolando et al., 2016), and  
204 mitochondrial-associated membranes, MAMs ((Escoll et al., 2017a). *LpSpl* encodes a  
205 sphingosine-1 phosphate (S1P) lyase that directly targets the host sphingolipid metabolism and  
206 restrains autophagy in infected cells. MitF (LegG1) activates the host small GTPase Ran to  
207 promote mitochondrial fragmentation during infection of human macrophages (Escoll et al.,  
208 2017b).

209 To learn if any of these effectors is involved in the T4SS-dependent induction of the “reverse  
210 mode” of the F<sub>0</sub>F<sub>1</sub>-ATPase, we infected hMDMs during 6 hours with Lpp-WT or its isogenic  
211 mutants lacking the T4SS (Lpp- $\Delta dotA$ ), lacking the effector LncP (Lpp- $\Delta lncP$ ), lacking the  
212 effector *LpSpl* (Lpp- $\Delta spl$ ), and *L. pneumophila* strain Philadelphia JR32 (JR32-WT) and its  
213 isogenic mutants lacking the T4SS (JR32- $\Delta icmT$ ) or the effector MitF (JR32- $\Delta mitF$ ). Using the  
214 TMRM high-content assay, we measured the  $\Delta\psi_m$  after the inhibition of the F<sub>0</sub>F<sub>1</sub>-ATPase by

215 DCCD (Figure 2H). Our results indicated that, while the  $F_0F_1$ -ATPase worked in the “forward  
216 mode” in non-infected hMDMs and during infection with T4SS-deficient mutants (*Lpp- $\Delta dotA$*   
217 and *JR32- $\Delta icmT$* ), the  $F_0F_1$ -ATPase worked in the “reverse mode” during infection with the  
218 *Lpp*-WT and *JR32*-WT strains (Figure 2G). Infection with *Lpp- $\Delta IncP$*  and *JR32- $\Delta mitF$*  were  
219 not significantly different compared to the WT strains, suggesting that these effectors are not  
220 involved in the induction of the “reverse mode” of the mitochondrial ATPase. However,  
221 mitochondria of cells infected with *Lpp- $\Delta spl$*  showed a significantly higher  $\Delta\psi_m$  after DCCD  
222 treatment than mitochondria of cells infected with *Lpp*-WT ( $p=0.0006$ ), and a significantly  
223 lower  $\Delta\psi_m$  after DCCD treatment than mitochondria of cells infected with the *Lpp- $\Delta dotA$*  strain  
224 ( $p=0.0034$ ). This suggests that *LpSpl* is partially involved in the induction of the “reverse mode”  
225 of the  $F_0F_1$ -ATPase, however other additional T4SS effector(s) seem to participate in the  
226 modulation of the  $F_0F_1$ -ATPase activity mode.

### 227 **Inhibition of *Legionella*-induced “Reverse Mode” Collapses the $\Delta\psi_m$ And Ignites Cell** 228 **Death of Infected Macrophages**

229 To further analyze the importance of the activity mode of the  $F_0F_1$ -ATPase during infection,  
230 we used BTB06584 (hereafter called BTB), a specific inhibitor of the “reverse mode” of the  
231 mitochondrial  $F_0F_1$ -ATPase (Ivanov et al., 2014). We used the TMRM high-content assay and  
232 added BTB to non-infected, *Lpp*-WT- or *Lpp- $\Delta dotA$* -infected hMDMs at 6 hpi. As shown in  
233 Figure 3A, the  $\Delta\psi_m$  collapsed specifically and significantly in WT infected cells (Figure 3B and  
234 3C) compared to non-infected ( $p=0.0022$ ) and  *$\Delta dotA$* -infected cells ( $p=0.0238$ ), further  
235 confirming that the  $F_0F_1$ -ATPase works in the “reverse mode” during WT infection. Indeed,  
236 the addition of BTB to *Lpp*-WT-infected hMDMs led to a significant reduction of the  $\Delta\psi_m$   
237 ( $p<0.0001$ ) at every time point post-infection (1-10 hpi) and at the single-cell level compared  
238 to non-treated *Lpp*-WT-infected cells (Figure 3D), further confirming that conservation of  $\Delta\psi_m$   
239 during *L. pneumophila* infection is caused by induction of  $F_0F_1$ -ATPase “reverse mode”.

240 As OXPHOS cessation and  $\Delta\psi_m$  collapse can trigger cell death, we reasoned that induction  
241 of the “reverse mode” of mitochondrial ATPase by *L. pneumophila* to maintain  $\Delta\psi_m$  in the  
242 absence of OXPHOS might delay cell death of infected cells. To test this hypothesis, we  
243 infected hMDMs with *Lpp*-WT and treated them with BTB or left them untreated, and then  
244 measured the percentage of living cells among infected cells (Figure 4A). Our results showed  
245 that the percentage of living, infected cells significantly decreased after 10 hpi in BTB-treated  
246 infected hMDMs compared to non-treated cells. As this reduction in the percentage of living,  
247 infected cells upon “reverse mode” inhibition might be caused by increased cell death, we used

248 our high-content assay to measure Annexin-V, a marker of early apoptosis, in a high number  
249 of living hMDMs during infection (Figure 4B and 4C). While addition of BTB during 24 hours  
250 did not increase the percentage of Annexin-V<sup>+</sup> cells in non-infected cells, the addition of this  
251 “reverse mode” inhibitor to Lpp-WT-infected hMDMs significantly increased the percentage  
252 of Annexin-V<sup>+</sup> cells compared to non-treated cells (p=0.0312). This suggests that the inhibition  
253 of the “reverse mode” by BTB leads to a reduction in the percentage of infected cells as  
254 increased cell death occurs specifically in infected cells. Single-cell analysis at 12 and 18 hpi  
255 (Figure 4D and S2A) also showed higher levels of Annexin-V intensity in BTB-treated Lpp-  
256 WT-infected hMDMs compared to non-treated infected cells (p<0.0001). BTB-treated infected  
257 cells also showed higher Hoechst nuclear levels compared to non-treated infected cells, a sign  
258 of nuclear condensation typical of apoptotic cells (Figure S2B), which further indicates that  
259 inhibition of the *Legionella*-induced ATPase “reverse mode” ignites cell death of infected  
260 macrophages. Taken together, our results suggest that the *Legionella*-induced “reverse mode”  
261 of the mitochondrial F<sub>0</sub>F<sub>1</sub>-ATPase aids to conserve  $\Delta\psi_m$  during infection to delay cell death of  
262 infected macrophages.

263 To simultaneously monitor  $\Delta\psi_m$  and early cell death signs in the same infected cell, we  
264 multiplexed Annexin-V and TMRM signals in our living cell assay (Figure 4E, S2C and S2D).  
265 *L. pneumophila*-infected macrophages where the “reverse mode” activity of the F<sub>0</sub>F<sub>1</sub>-ATPase  
266 was inhibited by BTB suffered a collapsed  $\Delta\psi_m$  and showed higher levels of Annexin-V at 12  
267 and 18 hpi (Figure 4E and S2D) compared to non-treated cells. Thus both events, collapse of  
268 the  $\Delta\psi_m$  and triggered cell death, occurred in the same infected cell when the *Legionella*-  
269 induced “reverse mode” activity of the F<sub>0</sub>F<sub>1</sub>-ATPase was inhibited. Furthermore, when the size  
270 of the bacterial vacuole was correlated with the  $\Delta\psi_m$  and cell death at the single-cell level (12  
271 and 18 hpi, Figure 4F and 4G respectively), intracellular bacterial replication occurred  
272 preferentially in those infected macrophages with intermediate levels of TMRM (non-collapsed  
273  $\Delta\psi_m$ ) and low Annexin-V levels (yellow color scale, Figure 4F and 4G), further indicating that  
274 conservation of  $\Delta\psi_m$  and delayed cell death are needed to guarantee the survival of infected  
275 macrophages to ensure bacterial replication.

## 276 DISCUSSION

277 We show here that by inducing the “reverse mode” of the mitochondrial F<sub>0</sub>F<sub>1</sub>-ATPase,  
278 *L. pneumophila* circumvents the collapse of  $\Delta\psi_m$  and cell death caused by OXPHOS cessation  
279 in infected cells. This mechanism, which partially involves the T4SS effector *LpSpl*, maintains  
280 the  $\Delta\psi_m$  and delays host cell death during infection, thus preserving bacterial replication niches

281 in conditions where mitochondrial respiration is abruptly reduced. Indeed, not only  
282 *L. pneumophila*, but also several other intracellular bacterial pathogens, such as  
283 *Mycobacterium tuberculosis* or *Chlamydia pneumoniae*, reduce mitochondrial OXPHOS  
284 during infection (Siegl et al., 2014; Singh et al., 2012)(Escoll and Buchrieser, 2019). OXPHOS  
285 reduction allows the pathogen to redirect cellular resources from mitochondria to the cytoplasm,  
286 which enhances glycolysis and biosynthetic pathways that can provide intracellular bacteria  
287 with resources needed for bacterial growth (Escoll and Buchrieser, 2018; Russell et al., 2019).  
288 In contrast, OXPHOS cessation in macrophages also enhances the biosynthetic pathways  
289 leading to the synthesis of cytokines and antimicrobial compounds (O’Neill and Pearce, 2016;  
290 Russell et al., 2019). Furthermore, OXPHOS reduction may trigger profound consequences for  
291 host cells, such as the collapse of  $\Delta\psi_m$  that may lead to subsequent cell death of infected cells.  
292 For macrophages, cell death is considered as a defense mechanism against infection (Chow et  
293 al., 2016). Indeed, pyroptosis of infected macrophages permits the spread of inflammatory  
294 mediators such as IL-1 $\beta$ . Thus, for intracellular bacteria, many of which infect macrophages  
295 (Mitchell et al., 2016), the death of their host cell is an obstacle as their cellular replication  
296 niche is destroyed. Therefore, while bacterial-induced reduction of OXPHOS might be  
297 beneficial for intracellular bacteria to obtain host cell resources, they need to counterbalance  
298 the consequences of OXPHOS cessation, i.e. the collapse of the mitochondrial  $\Delta\psi_m$  and  
299 subsequent cell death, to preserve their replication niches.

300 We have previously shown that the *L. pneumophila* T4SS effector MitF is implicated in  
301 fragmenting the mitochondrial networks of infected macrophages. These changes in the  
302 mitochondrial dynamics have a profound impact on OXPHOS that was severely impaired and  
303 accompanied by increased glycolysis in *Legionella*-infected cells (Escoll et al., 2017b). Here  
304 we show that, despite the impairment of mitochondrial respiration in infected cells,  
305 *L. pneumophila* conserves the  $\Delta\psi_m$  of host cells by inducing the “reverse mode” of the F<sub>o</sub>F<sub>1</sub>-  
306 ATPase by a mechanism that is T4SS-dependent and partially mediated by the T4SS effector  
307 *LpSpl*. When translocated into human cells, the S1P-lyase activity of *L. pneumophila* *LpSpl*  
308 reduces S1P levels in infected cells and restrains autophagy, likely because S1P is involved in  
309 the initiation of autophagosome formation at MAMs (Rolando et al., 2016).

310 How *LpSpl* may regulate the activity of the F<sub>o</sub>F<sub>1</sub>-ATPase is an interesting question. Indeed,  
311 phosphorylated lipids are critical regulators of mitochondrial functions and S1P is a potent lipid  
312 mediator that regulates various physiological processes as well as diverse mitochondrial  
313 functions such as mitochondrial respiration, ETC functioning or mitochondrial-dependent cell  
314 death (Hernández-Corbacho et al., 2017; Nielson and Rutter, 2018). Furthermore it was

315 reported that S1P interaction with Prohibitin 2 (PHB2) regulates ETC functioning and  
316 mitochondrial respiration (Strub et al., 2011) and that a link between PHB2, ETC functioning  
317 and the activation of “mitoflashes” (Jian et al., 2017) exists, which are dynamic and transient  
318 uncouplings of mitochondrial respiration from ATP production that are partially dependent on  
319 the “reverse mode” of the F<sub>o</sub>F<sub>1</sub>-ATPase (Wei-LaPierre and Dirksen, 2019). Thus, it is possible  
320 that *LpSpl* modulates mitochondrial S1P levels helping the induction of the “reverse mode” of  
321 the mitochondrial F<sub>o</sub>F<sub>1</sub>-ATPase by involving PHB2, ETC complex assembly or the generation  
322 of mitoflashes, a fascinating possibility that we will further investigate.

323 The regulation of host cell death by intracellular bacteria is widely studied (Rudel et al.,  
324 2010). For *L. pneumophila*, T4SS effectors activating and inhibiting cell death of infected cells  
325 have been described (Speir et al., 2014), suggesting that a very delicate interplay of positive  
326 and negative signals governs the fate of infected macrophages. Here we have shown that  
327 bacterial replication occurs preferentially in those infected macrophages that are able to  
328 conserve the  $\Delta\psi_m$  and delay cell death, a condition that is difficult to achieve in the absence of  
329 mitochondrial respiration. Thus, the manipulation of the activity of the mitochondrial F<sub>o</sub>F<sub>1</sub>-  
330 ATPase by *L. pneumophila*, which allows this pathogen to use the ATP hydrolase activity to  
331 pump H<sup>+</sup> to the IMS to maintain the  $\Delta\psi_m$  in infected cells, is a novel virulence strategy that  
332 might contribute to the fine-tuning of the timing of host cell death during bacterial infection.

## 333 **MATERIALS and METHODS**

### 334 **Human Primary Cell Cultures**

335 Human blood was collected from healthy volunteers under the ethical rules established by the  
336 French National Blood Service (EFS). Peripheral blood mononuclear cells (PBMCs) were  
337 isolated by Ficoll-Hypaque density-gradient separation (Lympholyte-H; Cedarlane  
338 Laboratories) at room temperature. PBMCs were incubated with anti-human CD14 antibodies  
339 coupled to magnetic beads (Miltenyi Biotec) and subjected to magnetic separation using LS  
340 columns (Miltenyi Biotec). Positive selected CD14<sup>+</sup> cells were counted and CD14 expression  
341 was analysed by flow cytometry, repeatedly showing a purity > 90%. CD14 cells were plated  
342 in RPMI 1640 medium (Life Technologies) supplemented with 10% heat-inactivated fetal  
343 bovine serum (FBS, Biowest) in 6 well multi-dish Nunc UpCell Surface cell culture plates or  
344 10 cm Nunc UpCell Surface cell culture dishes (Thermo Fisher) and differentiated to human  
345 monocyte-derived macrophages (hMDMs) by incubation with 100 ng/ml of recombinant  
346 human macrophage colony-stimulating factor (rhMCSF, Miltenyi Biotec) for 6 days at 37°C  
347 with 5% CO<sub>2</sub> in a humidified atmosphere. At day 3, additional rhMCSF (50 ng/ml) was added.

348 After 6 days differentiation, UpCell plates were placed at 20°C during 10 minutes and hMDMs  
349 were gently detached, counted and plated in RPMI 1640 10% FBS in 384-well plates (Greiner  
350 Bio-One).

### 351 **Bacterial strains and mutant construction**

352 *L. pneumophila* strain Paris or JR32 and their derivatives were grown for 3 days on N-(2-  
353 acetamido)-2-amino-ethanesulfonic acid (ACES)-buffered charcoal-yeast (BCYE) extract  
354 agar, at 37°C. For eGFP-expressing strains harbouring pNT28 plasmid (Tiaden et al., 2007),  
355 chloramphenicol (Cam; 5 µg/mL) was added. Knock-out mutant strains of *L. pneumophila*  
356 genes coding for the T4SS effectors *LpSpl* and *MitF/LegG1* were previously described (Escoll  
357 et al., 2017b; Rolando et al., 2016; Rothmeier et al., 2013). The knock-out mutant strain of the  
358 *L. pneumophila* gene coding for the effector *LncP* was constructed as previously described  
359 (Brüggemann et al., 2006; Rolando et al., 2016). In brief, the gene of interest was inactivated  
360 by introduction of an apramycine resistance (*apraR*) cassette into the chromosomal gene by 3-  
361 steps PCR. The g primers used for the *lncP* (*lpp2981*) knock out mutant are: *LncP\_F*:  
362 ACCCTGGTTCATGGTAACAATGG; *LncP\_Inv\_R*:  
363 GAGCGGATCGGGGATTGTCTTATCAGGCGAATGGTGTGAAAGG; *LncP\_Inv\_F*:  
364 GCTGATGGAGCTGCACATGAAACGTCATGGTCGTGCTGGTTG; *LncP\_R*:  
365 AATCAGATGGGTAAGCCGATTGG. To amplify the apramycine cassette, the primers  
366 *Apra\_F*: TTCATGTGCAGCTCCATCAGC and *Apra\_R*: AAGACAATCCCCGATCCGCTC  
367 were used.

### 368 **Infection of hMDMs and automatic confocal imaging**

369 hMDMs were infected with *L. pneumophila* grown for three days on BCYE agar plates.  
370 Bacteria were dissolved in 1X PBS (Life Technologies), the optical density (OD) was adjusted  
371 to OD<sub>600</sub> of 2.5 ( $2.2 \times 10^9$  bacteria/mL) and the bacteria were then further diluted in serum-free  
372 XVIVO-15 medium (Lonza) prior to infection to obtain the respective multiplicity of infection  
373 (MOI). hMDMs were washed twice with serum-free XVIVO-15 medium and then infected  
374 (MOI = 10) with 25 µL of bacteria in 384-well plates (Greiner Bio-One). The infection was  
375 synchronized by centrifugation (200 g for 5 min) and the infected cells were incubated at 37°C  
376 for 5 min in a water bath and then for 25 min at 37°C/5%CO<sub>2</sub>. After three intensive washes  
377 with serum-free XVIVO-15 medium, the infection proceeded in serum-free XVIVO-15  
378 medium for the respective time points. 30 min prior imaging, 25 µL of culture medium were  
379 removed and replaced by 25 µL of 2X mix of dyes, to a final concentration of 200 ng/mL of  
380 Hoechst H33342 (nuclear staining; Life Technologies), 10 nM of TMRM (mitochondrial

381 membrane potential; Life Technologies), and/or 1/100 Annexin-V-Alexa Fluor 647 (early  
382 apoptosis; Life Technologies). If chemical inhibitors of the Electron Transport Chain (ETC)  
383 were used in the experiments, they were added to hMDMs at the indicated times points at the  
384 following concentrations: 5  $\mu$ M Oligomycin (Enzo), 100  $\mu$ M DCCD  
385 (Dicyclohexylcarbodiimide, Sigma), 10  $\mu$ M FCCP (Tocris), 50  $\mu$ M BTB06584 (Sigma). Image  
386 acquisitions of multiple fields (9 to 25) per well were performed on an automated confocal  
387 microscope (OPERA Phenix, Perkin Elmer) using 60X objective, excitation lasers at 405, 488,  
388 561 and 640 nm, and emission filters at 450, 540, 600 and 690 nm, respectively.

### 389 **Metabolic Extracellular Flux Analysis**

390 hMDMs (50,000) were plated in XF-96-cell culture plates (Seahorse Bioscience). For OCR  
391 measurements, XF Assay Medium (Seahorse Bioscience) supplemented with 1 mM pyruvate  
392 and 10 mM glucose was used, and OCR was measured in a XF-96 Flux Analyzer (Seahorse  
393 Bioscience). For the mitochondrial respiratory control assay, hMDMs were infected at MOI =  
394 10 and at 6 hpi., different drugs were injected (Mitostress kit, Seahorse Bioscience) while OCR  
395 was monitored. Specifically, Olygomycin was injected through the port A, then FCCP was  
396 injected through the port B, and finally Rotenone + Antimycin A were injected through the port  
397 C, to reach each of the drugs a final concentration in the well of 0.5  $\mu$ M.

### 398 **Automatic High-Content Analyses (HCA)**

399 All analyses were performed with Harmony software v.4.9 (Perkin Elmer) using in-house  
400 developed scripts (available upon request). For the HCA of the mitochondrial membrane  
401 potential ( $\Delta\psi_m$ ), the Hoechst signal was used to segment nuclei in the 405/450 channel  
402 (excitation/emission), Hoechst background signal in the cytoplasm was used to segment the  
403 cytoplasm region in the 405/450 channel, *L. pneumophila* was identified by measuring the GFP  
404 signal in the 488/540 channel, and TMRM (10 nM) signal in the 561/600 channel was used to  
405 measure  $\Delta\psi_m$  by calculating SD/Mean TMRM intensity values in each infected and non-  
406 infected cell. For the HCA of cell death, the Hoechst signal was used to segment nuclei in the  
407 405/450 channel, Hoechst background signal in the cytoplasm was used to segment the  
408 cytoplasm region, and the identification of *L. pneumophila* was performed using the GFP signal  
409 in the 488/540 channel. Then, Annexin-V-AlexaFluor 647 signal was measured in the 640/690  
410 channel and the Hoechst signal intensity was measured in the 405/450 channel for each infected  
411 or non-infected cell. For the HCA analyses combining  $\Delta\psi_m$  and cell death, both HCA strategies  
412 aforementioned were merged, using high Hoechst signal in the 405/450 channel to segment  
413 nuclei, low Hoechst signal in the 405/450 channel to segment cytoplasm, GFP signal in the

414 488/540 channel to identify bacteria, TMRM signal in the 561/600 channel to measure  $\Delta\psi_m$   
415 (SD/Mean) and Annexin-V-AlexaFluor 647 signal in the 640/690 channel to measure cell  
416 death.

### 417 **Whole genome sequencing for mutant validation**

418 Chromosomal DNA was extracted from BCYE-grown *L. pneumophila* using the DNeasy Blood  
419 and Tissue Kit (Qiagen). The Illumina NGS libraries were prepared using the Nextera DNA  
420 Flex Library Prep following the manufacturer's instructions (Illumina Inc.). High-throughput  
421 sequencing was performed with a MiSeq Illumina sequencer ( $2 \times 300$  bp, Illumina Inc.) by the  
422 Biomics Pole (Institut Pasteur). For the analysis, we first removed adapters from Illumina  
423 sequencing reads using Cutadapt software version 1.15 (Martin, 2011) and we used Sickle  
424 (<https://github.com/najoshi/sickle>) with a quality threshold of 20 (Phred score) to trim bad  
425 quality extremities. Reads were assembled using Spades (Nurk et al., 2013) and different K-  
426 mer values. The region corresponding to the gene of interest was identified by blastn, extracted,  
427 and compared to the homologous region in the *L. pneumophila* strain Paris WT genome and to  
428 the antibiotic cassette sequence using blastn. The results are visually inspected with ACT  
429 (Artemis Comparison Tool) (Carver et al., 2005). In addition, we searched the entire genome  
430 whether off-target mutations had occurred, using Bowtie 2 (Langmead and Salzberg, 2012) to  
431 perform a mapping against the genome sequence of *L. pneumophila* strain Paris  
432 (NC\_006368.1). SNPs and small indels were searched for with freebayes SNP caller (Garrison  
433 and Marth, 2012), mutations and small indels were visualized in the Artemis genome viewer  
434 (Carver et al., 2005) to analyze them (new amino acid, synonymous mutation, frameshifts, etc).  
435 We used Samtools to find regions with no coverage (or close to zero) (Li et al., 2009). Regions  
436 or positions with such anomalies were visualized and compared with the corresponding region  
437 of the assembly. This confirmed that no off-target mutations impacting the phenotype of the  
438 mutant had occurred.

### 439 **Statistical analyses**

440 The two-sample Student's t-test (Mann-Whitney *U* test, non-assumption of Gaussian  
441 distributions) was used in all data sets unless stated otherwise. Data analysis was performed  
442 using Prism v9 (Graphpad Software).

### 443 **AUTHOR CONTRIBUTIONS**

444 PE conceived the study; PE, LP, MD and SS prepared blood-derived human cells and/or  
445 performed experiments; TS constructed bacterial mutants; PE, LP and CR analyzed data; PE  
446 and CB provided funding; CB provided critical advice; PE and CB wrote the manuscript.

## 447 ACKNOWLEDGEMENTS

448 We acknowledge C.B.'s, P. Glaser's lab members and F. Stavru at Institut Pasteur for fruitful  
449 discussions. We thank N. Aulner, A. Danckaert, Photonic BioImaging (PBI) UTechS and M.  
450 Hassan, Center for Translational Science (CRT) at Institut Pasteur, for support. This research  
451 was funded by the Institut Pasteur, DARRI - Institut Carnot - *Microbe et santé* (grant number  
452 INNOV-SP10-19) to PE; the Agence National de Recherche (grant number ANR-10-LABX-  
453 62-IBEID) and the Fondation de la Recherche Médicale (FRM) (grant number  
454 EQU201903007847) to CB, and the Région Ile-de-France (program DIM1Health) to PBI (part  
455 of FranceBioImaging, ANR-10-INSB-04-01). MD was supported by the Ecole Doctorale FIRE  
456 – “Programme Bettencourt”. SS was supported by the Pasteur Paris-University (PPU)  
457 International PhD Program.

## 458 REFERENCES

- 459 Bock FJ, Tait SWG. 2020. Mitochondria as multifaceted regulators of cell death. *Nat Rev Mol*  
460 *Cell Biol* **21**:85–100. doi:10.1038/s41580-019-0173-8
- 461 Brand MD, Nicholls DG. 2011. Assessing mitochondrial dysfunction in cells. *Biochem J*  
462 **435**:297–312. doi:10.1042/BJ20110162
- 463 Brüggemann H, Hagman A, Jules M, Sismeiro O, Dillies M-A, Gouyette C, Kunst F, Steinert  
464 M, Heuner K, Coppée J-Y, Buchrieser C. 2006. Virulence strategies for infecting  
465 phagocytes deduced from the in vivo transcriptional program of *Legionella*  
466 *pneumophila*. *Cell Microbiol* **8**:1228–1240. doi:10.1111/j.1462-5822.2006.00703.x
- 467 Carver TJ, Rutherford KM, Berriman M, Rajandream M-A, Barrell BG, Parkhill J. 2005. ACT:  
468 the Artemis Comparison Tool. *Bioinformatics* **21**:3422–3423.  
469 doi:10.1093/bioinformatics/bti553
- 470 Chow SH, Deo P, Naderer T. 2016. Macrophage cell death in microbial infections. *Cellular*  
471 *Microbiology* **18**:466–474. doi:https://doi.org/10.1111/cmi.12573
- 472 Connolly NMC, Theurey P, Adam-Vizi V, Bazan NG, Bernardi P, Bolaños JP, Culmsee C,  
473 Dawson VL, Deshmukh M, Duchen MR, Düssmann H, Fiskum G, Galindo MF,  
474 Hardingham GE, Hardwick JM, Jekabsons MB, Jonas EA, Jordán J, Lipton SA,  
475 Manfredi G, Mattson MP, McLaughlin B, Methner A, Murphy AN, Murphy MP,  
476 Nicholls DG, Polster BM, Pozzan T, Rizzuto R, Satrústegui J, Slack RS, Swanson RA,  
477 Swerdlow RH, Will Y, Ying Z, Joselin A, Gioran A, Moreira Pinho C, Watters O,  
478 Salvucci M, Llorente-Folch I, Park DS, Bano D, Ankarcrona M, Pizzo P, Prehn JHM.  
479 2018. Guidelines on experimental methods to assess mitochondrial dysfunction in  
480 cellular models of neurodegenerative diseases. *Cell Death Differ* **25**:542–572.  
481 doi:10.1038/s41418-017-0020-4
- 482 Degtyar E, Zusman T, Ehrlich M, Segal G. 2009. A *Legionella* effector acquired from protozoa  
483 is involved in sphingolipids metabolism and is targeted to the host cell mitochondria.  
484 *Cell Microbiol* **11**:1219–1235. doi:10.1111/j.1462-5822.2009.01328.x
- 485 Dolezal P, Aili M, Tong J, Jiang J-H, Marobbio CM, Lee S fung, Schuelein R, Belluzzo S,  
486 Binova E, Mousnier A, Frankel G, Giannuzzi G, Palmieri F, Gabriel K, Naderer T,  
487 Hartland EL, Lithgow T. 2012. *Legionella pneumophila* Secretes a Mitochondrial  
488 Carrier Protein during Infection. *PLoS Pathogens* **8**. doi:10.1371/journal.ppat.1002459

- 489 Duchen MR, Surin A, Jacobson J. 2003. [17] Imaging mitochondrial function in intact  
490 cells *Methods in Enzymology, Biophotonics, Part B*. Academic Press. pp. 353–389.  
491 doi:10.1016/S0076-6879(03)61019-0
- 492 Escoll P, Buchrieser C. 2019. Metabolic reprogramming: an innate cellular defence mechanism  
493 against intracellular bacteria? *Current Opinion in Immunology* **60**:117–123.  
494 doi:10.1016/j.coi.2019.05.009
- 495 Escoll P, Buchrieser C. 2018. Metabolic reprogramming of host cells upon bacterial infection:  
496 Why shift to a Warburg-like metabolism? *FEBS J* **285**:2146–2160.  
497 doi:10.1111/febs.14446
- 498 Escoll P, Rolando M, Buchrieser C. 2017a. MAMs are attractive targets for bacterial  
499 repurposing of the host cell: MAM-functions might be key for undermining an infected  
500 cell. *Bioessays* **39**. doi:10.1002/bies.201600171
- 501 Escoll P, Song O-R, Viana F, Steiner B, Lagache T, Olivo-Marin J-C, Impens F, Brodin P,  
502 Hilbi H, Buchrieser C. 2017b. Legionella pneumophila Modulates Mitochondrial  
503 Dynamics to Trigger Metabolic Repurposing of Infected Macrophages. *Cell Host &*  
504 *Microbe* **22**:302-316.e7. doi:10.1016/j.chom.2017.07.020
- 505 Gandhi S, Wood-Kaczmar A, Yao Z, Plun-Favreau H, Deas E, Klupsch K, Downward J,  
506 Latchman DS, Tabrizi SJ, Wood NW, Duchen MR, Abramov AY. 2009. PINK1-  
507 Associated Parkinson’s Disease Is Caused by Neuronal Vulnerability to Calcium-  
508 Induced Cell Death. *Molecular Cell* **33**:627–638. doi:10.1016/j.molcel.2009.02.013
- 509 Garrison E, Marth G. 2012. Haplotype-based variant detection from short-read sequencing.  
510 *arXiv:12073907 [q-bio]*.
- 511 Hernández-Corbacho MJ, Salama MF, Canals D, Senkal CE, Obeid LM. 2017. Sphingolipids  
512 in mitochondria. *Biochimica et Biophysica Acta (BBA) - Molecular and Cell Biology of*  
513 *Lipids* **1862**:56–68. doi:10.1016/j.bbalip.2016.09.019
- 514 Ivanec F, Faccenda D, Gatliff J, Ahmed AA, Cocco S, Cheng CHK, Allan E, Russell C, Duchen  
515 MR, Campanella M. 2014. The compound BTB06584 is an IF1-dependent selective  
516 inhibitor of the mitochondrial F1Fo-ATPase. *British Journal of Pharmacology*  
517 **171**:4193–4206. doi:10.1111/bph.12638
- 518 Jian C, Xu F, Hou T, Sun T, Li J, Cheng H, Wang X. 2017. Deficiency of PHB complex impairs  
519 respiratory supercomplex formation and activates mitochondrial flashes. *J Cell Sci*  
520 **130**:2620–2630. doi:10.1242/jcs.198523
- 521 Langmead B, Salzberg SL. 2012. Fast gapped-read alignment with Bowtie 2. *Nat Methods*  
522 **9**:357–359. doi:10.1038/nmeth.1923
- 523 Li H, Handsaker B, Wysoker A, Fennell T, Ruan J, Homer N, Marth G, Abecasis G, Durbin R,  
524 1000 Genome Project Data Processing Subgroup. 2009. The Sequence Alignment/Map  
525 format and SAMtools. *Bioinformatics* **25**:2078–2079.  
526 doi:10.1093/bioinformatics/btp352
- 527 Martin M. 2011. Cutadapt removes adapter sequences from high-throughput sequencing reads.  
528 *EMBnet.journal* **17**:10–12. doi:10.14806/ej.17.1.200
- 529 Mitchell G, Chen C, Portnoy DA. 2016. Strategies Used by Bacteria to Grow in Macrophages.  
530 *Microbiology Spectrum* **4**. doi:10.1128/microbiolspec.MCHD-0012-2015
- 531 Mondino S, Schmidt S, Rolando M, Escoll P, Gomez-Valero L, Buchrieser C. 2020.  
532 Legionnaires’ Disease: State of the Art Knowledge of Pathogenesis Mechanisms of  
533 Legionella. *Annu Rev Pathol Mech Dis* **15**:439–466. doi:10.1146/annurev-  
534 pathmechdis-012419-032742
- 535 Nielson JR, Rutter JP. 2018. Lipid-mediated signals that regulate mitochondrial biology. *J Biol*  
536 *Chem* **293**:7517–7521. doi:10.1074/jbc.R117.001655
- 537 Nurk S, Bankevich A, Antipov D, Gurevich AA, Korobeynikov A, Lapidus A, Prjibelski AD,  
538 Pyshkin A, Sirotkin A, Sirotkin Y, Stepanauskas R, Clingenpeel SR, Woyke T, McLean  
539 JS, Lasken R, Tesler G, Alekseyev MA, Pevzner PA. 2013. Assembling single-cell

- 540 genomes and mini-metagenomes from chimeric MDA products. *J Comput Biol* **20**:714–  
541 737. doi:10.1089/cmb.2013.0084
- 542 O’Neill LAJ, Pearce EJ. 2016. Immunometabolism governs dendritic cell and macrophage  
543 function. *J Exp Med* **213**:15–23. doi:10.1084/jem.20151570
- 544 Rolando M, Escoll P, Nora T, Botti J, Boitez V, Bedia C, Daniels C, Abraham G, Stogios PJ,  
545 Skarina T, Christophe C, Dervins-Ravault D, Cazalet C, Hilbi H, Rupasinghe TWT,  
546 Tull D, McConville MJ, Ong SY, Hartland EL, Codogno P, Levade T, Naderer T,  
547 Savchenko A, Buchrieser C. 2016. Legionella pneumophila S1P-lyase targets host  
548 sphingolipid metabolism and restrains autophagy. *Proc Natl Acad Sci USA* **113**:1901–  
549 1906. doi:10.1073/pnas.1522067113
- 550 Rothmeier E, Pfaffinger G, Hoffmann C, Harrison CF, Grabmayr H, Repnik U, Hannemann M,  
551 Wölke S, Bausch A, Griffiths G, Müller-Taubenberger A, Itzen A, Hilbi H. 2013.  
552 Activation of Ran GTPase by a Legionella effector promotes microtubule  
553 polymerization, pathogen vacuole motility and infection. *PLoS Pathog* **9**:e1003598.  
554 doi:10.1371/journal.ppat.1003598
- 555 Rudel T, Kepp O, Kozjak-Pavlovic V. 2010. Interactions between bacterial pathogens and  
556 mitochondrial cell death pathways. *Nat Rev Microbiol* **8**:693–705.  
557 doi:10.1038/nrmicro2421
- 558 Russell DG, Huang L, VanderVen BC. 2019. Immunometabolism at the interface between  
559 macrophages and pathogens. *Nat Rev Immunol* **19**:291–304. doi:10.1038/s41577-019-  
560 0124-9
- 561 Siegl C, Prusty BK, Karunakaran K, Wischhusen J, Rudel T. 2014. Tumor Suppressor p53  
562 Alters Host Cell Metabolism to Limit Chlamydia trachomatis Infection. *Cell Reports*  
563 **9**:918–929. doi:10.1016/j.celrep.2014.10.004
- 564 Singh V, Jamwal S, Jain R, Verma P, Gokhale R, Rao KVS. 2012. Mycobacterium tuberculosis-  
565 Driven Targeted Recalibration of Macrophage Lipid Homeostasis Promotes the Foamy  
566 Phenotype. *Cell Host & Microbe* **12**:669–681. doi:10.1016/j.chom.2012.09.012
- 567 Speir M, Vince JE, Naderer T. 2014. Programmed cell death in Legionella infection. *Future*  
568 *Microbiology* **9**:107–118. doi:10.2217/fmb.13.139
- 569 Spier A, Stavru F, Cossart P. 2019. Interaction between Intracellular Bacterial Pathogens and  
570 Host Cell Mitochondria. *Microbiology Spectrum* **7**:BAI-0016-2019.
- 571 Strub GM, Paillard M, Liang J, Gomez L, Allegood JC, Hait NC, Maceyka M, Price MM, Chen  
572 Q, Simpson DC, Kordula T, Milstien S, Lesnefsky EJ, Spiegel S. 2011. Sphingosine-1-  
573 phosphate produced by sphingosine kinase 2 in mitochondria interacts with prohibitin  
574 2 to regulate complex IV assembly and respiration. *FASEB j* **25**:600–612.  
575 doi:10.1096/fj.10-167502
- 576 Tiaden A, Spirig T, Weber SS, Brüggemann H, Bosshard R, Buchrieser C, Hilbi H. 2007. The  
577 Legionella pneumophila response regulator LqsR promotes host cell interactions as an  
578 element of the virulence regulatory network controlled by RpoS and LetA. *Cell*  
579 *Microbiol* **9**:2903–2920. doi:10.1111/j.1462-5822.2007.01005.x
- 580 Wei-LaPierre L, Dirksen RT. 2019. Isolating a reverse-mode ATP synthase-dependent  
581 mechanism of mitoflash activation. *Journal of General Physiology* **151**:708–713.  
582 doi:10.1085/jgp.201912358

583

584

## 585 FIGURE LEGENDS

586 **Figure 1. Despite a reduction of oxidative phosphorylation (OXPHOS), hMDMs maintain**  
587 **their  $\Delta\psi_m$  during infection by *L. pneumophila*.** (A) hMDMs were infected with  
588 *L. pneumophila* strain Paris (Lpp) wild-type (WT), a T4SS-deficient  $\Delta dotA$  mutant, or left  
589 uninfected (Non-infected). At 6 hours post-infection (hpi), a cellular respiratory control assay  
590 was performed by measuring oxygen consumption rate (OCR) during the sequential addition  
591 of mitochondrial respiratory inhibitors (see also Figure S1A). (B) Basal respiration of hMDMs  
592 in the same conditions as in (A), at 6 hpi. (C) hMDMs were infected as in (A) with GFP-  
593 expressing bacteria (green), nuclei of host cells were stained with Hoechst (Nuc, blue) and  $\Delta\psi_m$   
594 was monitored from 1 to 12 hpi using TMRM dye in non-quenching conditions (10 nM).  
595 Representative confocal microscope images of non-infected and infected cells at 3, 6, 9 and 12  
596 hpi are shown. Intracellular bacterial replication can be observed in Lpp-WT infected hMDMs  
597 at 12 hpi. Bar: 20  $\mu\text{m}$ . (D) Quantification of TMRM intensity at 1-10 hpi (expressed as  
598 SD/Mean) in the assays described in (C). Data from 4 independent experiments with a total of  
599 10 replicates (E) Single-cell analysis at 6 hpi of the assays described in (C). Single-cell data  
600 from a representative experiment (full time-course in Figure S1C) \*\*p-value < 0.01; \*\*\*\*p-  
601 value < 0.00001; ns = non-significant (Mann-Whitney *U* test).

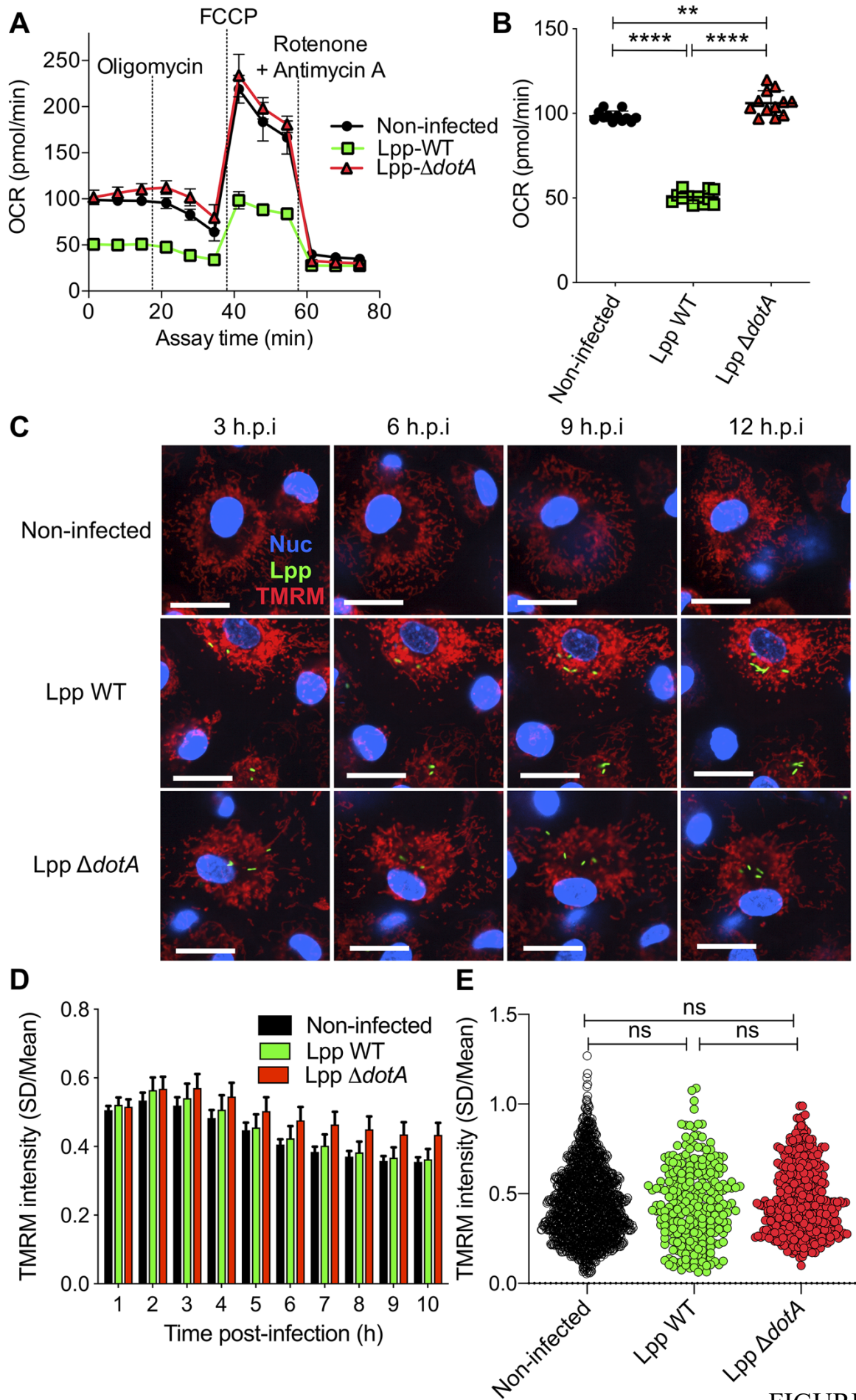
602 **Figure 2. The mitochondrial  $F_0F_1$ -ATPase works in the “reverse mode” during infection**  
603 **of hMDMs by *L. pneumophila*.** (A) In the “forward mode” of the mitochondrial ATPase, the  
604  $\Delta\psi_m$  generated by the Electron Transport Chain is used by the  $F_0F_1$ -ATPase to synthesize ATP.  
605 The “reverse mode” of the  $F_0F_1$ -ATPase leads to ATP hydrolysis to pump  $H^+$  to the  
606 intermembrane space (IMS). IMM: inner mitochondrial membrane. (B) When the  $F_0F_1$ -ATPase  
607 is inhibited by Oligomycin or DCCD, an increase in  $\Delta\psi_m$  indicates that the ATPase was  
608 working in the “forward mode” ( $H^+$  accumulate in the IMS), while a decrease in  $\Delta\psi_m$  indicates  
609 functioning in the “reverse mode” ( $H^+$  cannot be translocated to the IMS by the  $F_0F_1$ -ATPase  
610 to sustain the  $\Delta\psi_m$ ). (C) hMDMs were infected with GFP-expressing bacteria (green), or left  
611 uninfected (Non-infected). At 5.5 hpi cells were labeled with Hoechst to identify the cell  
612 nucleus (Nuc, blue) and TMRM (red) to quantify  $\Delta\psi_m$ . At 6 hpi, addition of medium (no  
613 changes) or FCCP (complete depolarization) was used as controls. Representative confocal  
614 images of Lpp-WT-infected hMDMs (6 hpi) at 5 min before the addition of medium (top) or  
615 FCCP (bottom), and at 5, 25 and 50 min after addition of medium or FCCP. Bar: 20  $\mu\text{m}$ . (D)  
616 Quantification of (C) before (baseline) and after the addition of medium. Each dot represents  
617 mean  $\pm$  SD of 3 independent experiments with a total of 8 replicates. (E) Same as (D) but FCCP

618 was added. **(F)** Same as (D) but oligomycin was added. **(G)** Same as (D) but DCCD was added.  
619 **(H)** Same as (C) but infection was performed with Lpp-WT, Lpp- $\Delta dotA$ , Lpp- $\Delta incP$ , Lpp- $\Delta spl$ ,  
620 *L. pneumophila* strain Philadelphia JR32 (JR32)-WT, JR32- $\Delta icmT$  or JR32- $\Delta mitF$ . TMRM  
621 values (SD/Mean) at 50 min after DCCD addition are shown. Data from a minimum of 3  
622 experiments per strain with 10 or more replicates per strain \*\*p-value < 0.01; \*\*\*p-value <  
623 0.001; \*\*\*\*p-value < 0.00001; ns = non-significant (Mann-Whitney *U* test)

624 **Figure 3. Inhibition of the “reverse mode” of mitochondrial F<sub>0</sub>F<sub>1</sub> ATPase reduces the  $\Delta\psi_m$**   
625 **of *L. pneumophila*-infected hMDMs. (A)** hMDMs were infected with GFP-expressing  
626 bacteria (green), Lpp-WT or Lpp- $\Delta dotA$ , or left uninfected (Non-infected). At 5.5 hpi cells were  
627 labeled with Hoechst to identify cell nucleus (Nuc, blue) and TMRM (red) to quantify  $\Delta\psi_m$ . At  
628 6 hpi, BTB06584 (BTB, 50  $\mu$ M), a specific inhibitor of the “reverse mode” of the ATPase, was  
629 added and  $\Delta\psi_m$  monitored. Representative confocal microscopy images of non-infected (top)  
630 and Lpp-WT-infected (bottom) hMDMs (6 hpi) at 5 min before the addition and at 5, 25 and  
631 50 min after the addition of BTB. Bar: 20  $\mu$ m. **(B)** Quantification of (C) before (baseline) and  
632 after the addition of BTB. Each dot represents the mean  $\pm$  SD of 3 independent experiments  
633 with a total of 6 replicates. **(C)** Same infection conditions than (A) but TMRM values  
634 (SD/Mean) at 50 min after BTB addition are shown. Data from 3 experiments with a total of 6  
635 replicates (3 replicates for Lpp- $\Delta dotA$ ) **(D)** Single-cell analysis of  $\Delta\psi_m$  in Lpp-WT-infected  
636 hMDMs treated with BTB (50  $\mu$ M) or left untreated (non-treated). Single-cell data from one  
637 representative experiment \*p-value < 0.05; \*\*p-value < 0.01; ns = non-significant (Mann-  
638 Whitney *U* test)

639 **Figure 4. Inhibition of F<sub>0</sub>-F<sub>1</sub> ATPase “reverse mode” increases cell death in**  
640 ***L. pneumophila*-infected hMDMs. (A)** hMDMs were infected with Lpp-WT-GFP and were  
641 non-treated or treated with 50  $\mu$ M BTB. The presence of GFP-expressing bacteria in each cell  
642 was monitored and the number of infected cells in the whole population was graphed as  
643 percentage of infected cells. Data from 3 independent experiments with a total of 7 replicates  
644 per condition and time-point **(B)** hMDMs were infected with Lpp-WT-GFP (green), the nuclei  
645 of host cells were stained with Hoechst (Nuc, blue) and Annexin-V Alexa Fluor 647 was added  
646 to the cell culture to monitor early cell death (Annexin, yellow) from 1 to 18 hpi in non-treated  
647 or BTB-treated hMDMs. Representative confocal images of non-treated and Lpp-WT-GFP-  
648 infected cells at 6, 12 and 18 hpi are shown. Intracellular bacterial replication can be observed  
649 in non-treated Lpp-WT infected hMDMs at 12 and 18 hpi. Bar: 20  $\mu$ m. **(C)** hMDMs stained as

650 in (B) were infected with Lpp-WT-GFP or left uninfected (Non-infected), and then were treated  
651 or not with BTB (50  $\mu$ M). Percentage of Annexin-V<sup>+</sup> cells at 24 hpi is shown. Data from 3  
652 independent experiments with a total of 7 replicates per condition **(D)** Single-cell analysis (12  
653 hpi) of Annexin-V intensity of the assays described in (B). Single-cell data from one  
654 representative experiment (18 hpi shown in Figure S2A) **(E)** hMDMs were infected with Lpp-  
655 WT-GFP, nuclei of host cells were stained with Hoechst, and TMRM and Annexin-V Alexa  
656 Fluor 647 were added to the cells to simultaneously monitor (1-18 hpi)  $\Delta\psi_m$  and early cell death,  
657 respectively, in non-treated or BTB-treated hMDMs (representative multi-field confocal  
658 images in Figure S2C). Single-cell analyses (12 hpi) of  $\Delta\psi_m$  (TMRM SD/Mean) and cell death  
659 (Annexin-V intensity) in more than 1600 cells per condition are shown. Single-cell data from  
660 one representative experiment; Green dots: Non-treated Lpp-WT-infected single cells. Orange  
661 dots: BTB-treated Lpp-WT-infected single cells. **(F)** Same infection conditions as in (E) but  
662 vacuole size was monitored in each Lpp-WT-infected single cell. Single-cell analyses (12 hpi)  
663 of  $\Delta\psi_m$  (TMRM SD/Mean), vacuole size ( $\mu\text{m}^2$ ), and cell death (Annexin-V intensity) in more  
664 than 3800 cells are shown. Single-cell data from one representative experiment; Color scale  
665 (yellow) represents Annexin V intensity per cell (AU). **(G)** Same as in (F) at 18 hpi. \*p-value  
666 < 0.05; \*\*p-value < 0.01; \*\*\*p-value < 0.001; \*\*\*\*p-value < 0.00001; ns = non-significant  
667 (Mann-Whitney *U* test)



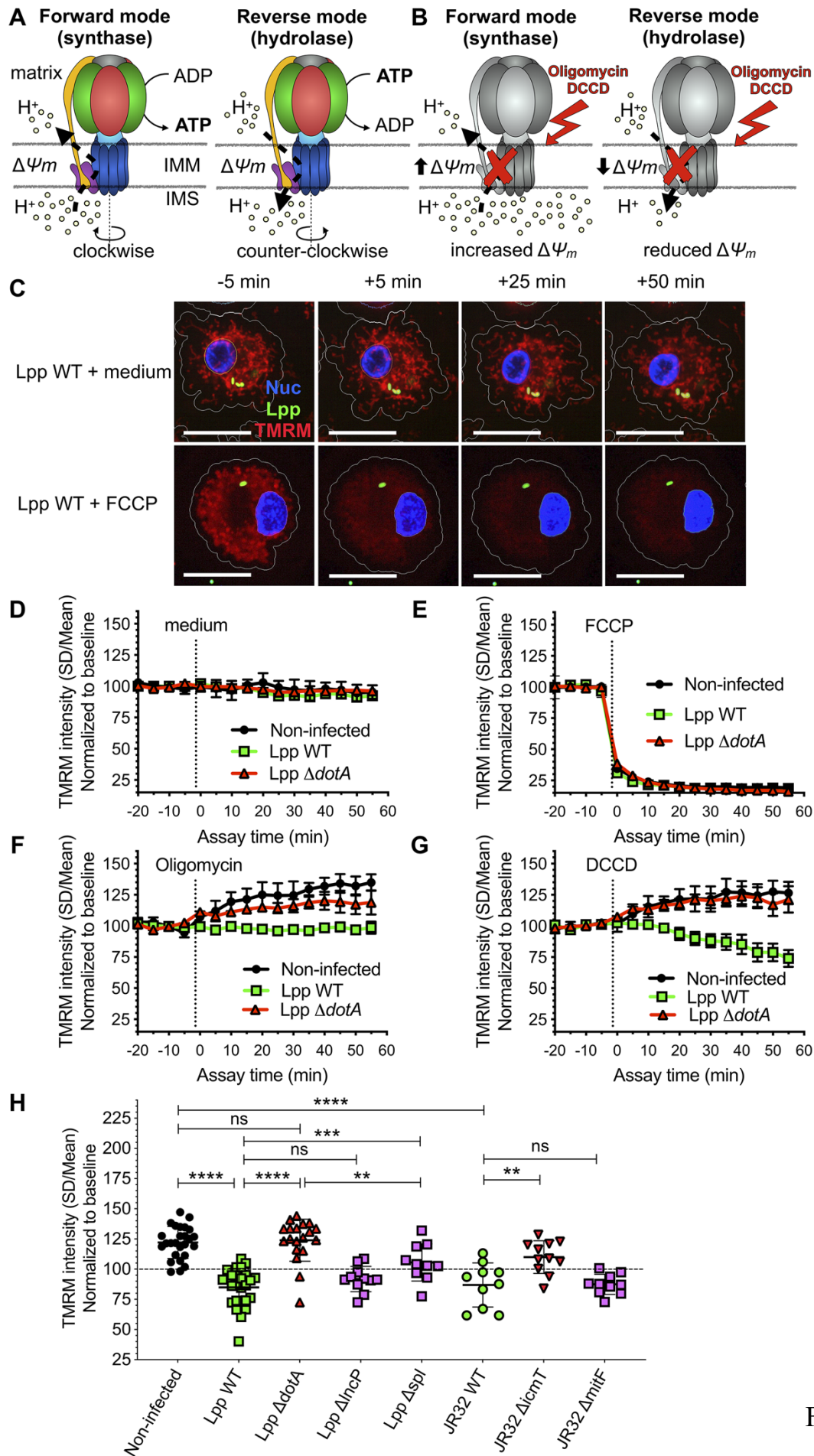
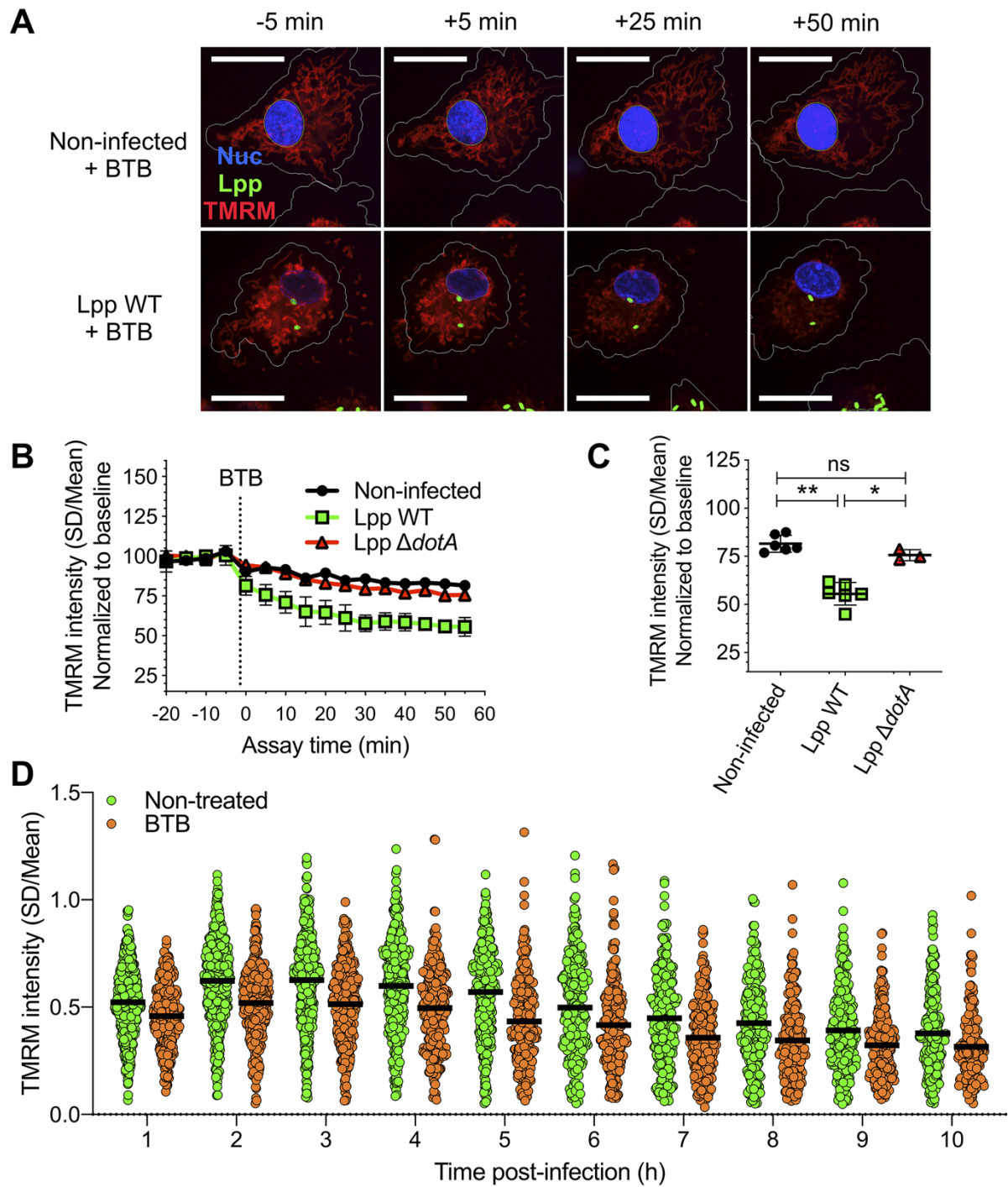


FIGURE 2



670

FIGURE 3

